

# Centrality Dependence of Thermal Parameters Deduced from Hadron Multiplicities in Au + Au Collisions at

$$\sqrt{s_{NN}} = 130 \text{ GeV}$$

J. CLEYMANS<sup>a</sup>, B. KÄMPFER<sup>b</sup>, M. KANETA<sup>c</sup>, S. WHEATON<sup>a</sup>, N. XU<sup>d</sup>

<sup>a</sup> *Department of Physics,*

*University of Cape Town,*

*Rondebosch 7701,*

*Cape Town, South Africa*

<sup>b</sup> *Institut für Kern- und Hadronenphysik,*

*Forschungszentrum Rossendorf,*

*PF 510119, D-01314 Dresden, Germany*

<sup>c</sup> *RIKEN BNL Research Center,*

*Brookhaven National Laboratory,*

*Upton, New York 11973*

<sup>d</sup> *Lawrence Berkeley National Laboratory,*

*Berkeley, California 94720*

## Abstract

We analyse the centrality dependence of thermal parameters deduced from hadron multiplicities in Au + Au collisions at  $\sqrt{s_{NN}} = 130 \text{ GeV}$ . While the chemical freeze-out temperature and chemical potentials are found to be roughly centrality-independent, the strangeness saturation factor  $\gamma_S$  increases with participant number towards unity, supporting the assumption of equilibrium freeze-out conditions in central collisions.

## I. INTRODUCTION

Statistical-thermal models (cf. [1] for recent surveys and references therein) have enjoyed remarkable success in describing hadron multiplicities observed in both heavy-ion and elementary collisions over a wide range of energies [2, 3, 4, 5, 6]. The final state multiplicities are reproduced in these models with very few parameters. The prominent ones are the chemical freeze-out temperature  $T$  and baryon chemical potential  $\mu_B$ . There are further chemical potentials to be considered below. A compilation of the freeze-out parameters over the accessible range of energies reveals a continuous curve in the  $T - \mu_B$  plane which may be characterized by an energy per hadron of the order of 1  $GeV$  [4]. While the occurrence of such a universal freeze-out curve is interesting in itself and is useful for extrapolations and interpolations as well, its particular meaning could be the approximate coincidence with the confinement border line, at least at high energies, as conjectured in [7].

We do not touch here on the disputed question as to why also the multiplicities of the rare multi-strange hadrons seem to obey chemical equilibrium (see [8]). Instead, we focus on one possible indicator of incomplete equilibrium, the strangeness saturation factor  $\gamma_s$ . This factor has been introduced [9] to account for an apparent under-saturation of strange hadrons. Various previous analyses [10] considered such a factor as necessary to accomplish a satisfactory description of data. For SPS energies,  $\sqrt{s_{NN}} = 6 \cdots 20 \text{ GeV}$ , it has been shown [11] that  $\gamma_s$  grows with increasing beam energy and centrality. First attempts [12], based on very restricted data sets, find also at RHIC energies a preliminary indication of rising  $\gamma_s$  with increasing centrality. It is the subject of this paper to investigate in detail the dependence of the thermal parameters including  $\gamma_s$  on the centrality in collisions of Au+Au at  $\sqrt{s_{NN}} = 130 \text{ GeV}$ . By now there is a sufficiently large basis of published data at this energy to allow a thorough analysis.

Our paper is organized as follows. In section II we recall the formulation of our employed statistical-thermal model. The analysed data are listed in section III. Our fit procedures are described in section IV and results are presented in section V. The summary and conclusions can be found in section VI.

## II. STATISTICAL-THERMAL MODEL

For suitably large systems at RHIC collider energies, hadron multiplicities are analysed by employing the grand-canonical partition function  $\mathcal{Z}(V, T, \mu_i) = \text{Tr} \left[ \exp\{-(\hat{H} - \sum_i \mu_i Q_i)/T\} \right]$ , where  $\hat{H}$  is the statistical operator of the system,  $T$  denotes the temperature, and  $\mu_i$  and  $Q_i$  are respectively the chemical potentials and corresponding conserved charges in the system. To be specific, we use here the baryon charge (corresponding to  $\mu_B$ ) and the strangeness charge (corresponding to  $\mu_S$ ) as unconstrained quantities. (There are other possible chemical potentials, e.g.,  $\mu_Q$  as electric charge potential. However, we put  $\mu_Q = 0$  with the reasoning explained below.)

The primordial particle numbers are accordingly,

$$N_i^{\text{prim}} = V g_i \int \frac{d^3 p}{(2\pi)^3} dm_i \left[ \gamma_s^{-|S_i|} e^{\frac{E_i - \mu_i Q_i}{T}} \pm 1 \right]^{-1} \text{BW}(m_i), \quad (2.1)$$

where we include phenomenologically the strangeness saturation factor  $\gamma_s$  (with  $|S_i|$  the total number of strange and anti-strange quarks in hadron species  $i$ ) to account for the possibility of incomplete equilibration in this sector;  $E_i = \sqrt{p^2 + m_i^2}$  and  $\text{BW}(m_i)$  is the Breit-Wigner distribution (to be replaced by a  $\delta$ -function for stable hadrons) to be integrated from thresholds with appropriate widths  $\Gamma_i$  (in practice the interval  $[\max\{\text{threshold}, m_i - 2\Gamma_i\}, m_i + 2\Gamma_i]$  is sufficient). The fiducial volume  $V$  drops in particle ratios.  $g_i$  is the degeneracy factor of particle species  $i$  with vacuum mass  $m_i$ . (The study of the effect of in-medium masses (cf. [13]) is interesting because it might shed light on the chiral properties of the medium created in heavy-ion collisions at RHIC.) Eq. (2.1) simplifies in the Boltzmann approximation (i.e., discarding the spin-statistics factor  $\pm 1$ ) and when neglecting the energy distribution of resonances. We use here the full expression Eq. (2.1) and include all hadron states with  $u, d, s$  quarks and corresponding anti-quarks up to 1.7 or 2.6  $GeV$  [32] with masses and total widths according to the particle data group listing [14]. The final particle numbers to be compared with experiment are  $N_i = N_i^{\text{prim}} + \sum_j \text{Br}^{j \rightarrow i} N_j^{\text{prim}}$  due to decays of unstable particles with branching ratios  $\text{Br}^{j \rightarrow i}$ .

Originally, such a description was thought to be justified for multiplicities measured over the entire phase-space, since many dynamical effects cancel out in ratios of hadron yields [5]. At sufficiently high energy, such as at RHIC, however, ratios

of mid-rapidity yields are also found to be well described by the statistical-thermal model [1, 3, 12, 15, 16].

### III. THE DATA

In contrast to SPS energies, where both mid-rapidity and fully phase space integrated data are at our disposal (see [12] for a comparison), at RHIC energy of  $\sqrt{s_{NN}} = 130 \text{ GeV}$  sufficiently many data of identified hadrons are available only at mid-rapidity. The data analysed here were compiled from PHENIX, PHOBOS, BRAHMS and STAR experimental results. These experiments differ in their cuts on the data. It turns out that the results for the deduced thermal freeze-out parameters depend in some cases sensitively on the employed data sets. Therefore, for definiteness Table I lists the ratios used as a function of collision centrality after recalculation to a common centrality binning as in [15]. Subscript "(1)" denotes yields corrected for weak feed-down, while yields labelled by "(2)" include a contribution from weak decays. Three centrality bins were selected with participant numbers  $63.5 \pm 8.4$  (peripheral),  $210.5 \pm 8.4$  (mid-central) and  $317.0 \pm 8.2$  (central).

### IV. THE FIT PROCEDURES

According to our propositions,  $T, \mu_B, \mu_S$  and  $\gamma_s$  are unconstrained fit parameters. For each centrality class, four fits were performed:

Fit I: all available ratios listed in Table I included;

Fit II: only ratios of  $\pi, K, p, \Lambda$  and  $\Xi$  included;

Fit III: only ratios of  $\pi, K, p$  and  $\Lambda$  included;

Fit IV: only ratios of  $\pi, K$  and  $p$  included.

In this way, the effect of the various multiplicities on the thermal parameters are investigated. (Various other fitting procedures are considered in [15].)

The final ratios compared with experiment include both a primordial and a decay contribution. As mentioned above, in some cases the experimental data have been corrected for weak decays. However, where such corrections have not been made, the influence of weak decays is included in the following way:

TABLE I: Ratios of hadrons in  $Au + Au$  collisions at  $\sqrt{s_{NN}} = 130$   $GeV$  from various RHIC experiments.

Ratio	Experiment	Central	Mid-Central	Peripheral
$\pi_{(2)}^-/\pi_{(2)}^+$	BRAHMS [19]	$0.990 \pm 0.100$		
	PHENIX [20, 21]	$0.960 \pm 0.177$	$0.920 \pm 0.170$	$0.933 \pm 0.172$
	PHOBOS [22]	$1.000 \pm 0.022$		
	STAR [17]	$1.000 \pm 0.073$	$1.000 \pm 0.073$	$1.000 \pm 0.073$
$K_{(2)}^+/K_{(2)}^-$	PHENIX [20, 21]	$1.152 \pm 0.240$	$1.292 \pm 0.268$	$1.322 \pm 0.284$
	PHOBOS [22]	$1.099 \pm 0.111$		
	STAR [23]	$1.109 \pm 0.022$	$1.105 \pm 0.036$	$1.120 \pm 0.040$
$\bar{p}_{(1)}/p_{(1)}$	PHENIX [20, 21]	$0.680 \pm 0.149$	$0.671 \pm 0.142$	$0.717 \pm 0.157$
$\bar{p}_{(2)}/p_{(2)}$	BRAHMS [19]	$0.650 \pm 0.092$		
	PHOBOS [22]	$0.600 \pm 0.072$		
	STAR [26]	$0.714 \pm 0.050$	$0.724 \pm 0.050$	$0.764 \pm 0.053$
$\bar{\Lambda}_{(1)}/\Lambda_{(1)}$	PHENIX [21]	$0.750 \pm 0.180$	$0.798 \pm 0.197$	$0.795 \pm 0.197$
$\bar{\Lambda}_{(2)}/\Lambda_{(2)}$	STAR [18]	$0.719 \pm 0.090$	$0.739 \pm 0.092$	$0.744 \pm 0.100$
$\bar{\Xi}_{(2)}^+/\Xi_{(2)}^-$	STAR [28, 29]	$0.840 \pm 0.053$	$0.822 \pm 0.114$	$0.815 \pm 0.096$
$\bar{\Omega}^+/\Omega^-$	STAR [29, 30]	$1.062 \pm 0.410$		
$K_{(2)}^-/\pi_{(2)}^-$	PHENIX [20, 21]	$0.151 \pm 0.030$	$0.134 \pm 0.027$	$0.116 \pm 0.023$
	STAR [17, 23]	$0.151 \pm 0.022$	$0.147 \pm 0.022$	$0.130 \pm 0.019$
$K_S^0/\pi_{(2)}^-$	STAR [17, 23]	$0.134 \pm 0.022$	$0.131 \pm 0.022$	$0.108 \pm 0.018$
$\bar{p}_{(1)}/\pi_{(2)}^-$	PHENIX [20, 21]	$0.049 \pm 0.010$	$0.047 \pm 0.010$	$0.045 \pm 0.009$
$\bar{p}_{(2)}/\pi_{(2)}^-$	STAR [17, 25]	$0.069 \pm 0.019$	$0.067 \pm 0.019$	$0.067 \pm 0.019$
$\Lambda_{(1)}/\pi_{(2)}^-$	STAR [17, 18]	$0.043 \pm 0.008$	$0.043 \pm 0.008$	$0.039 \pm 0.007$
$\Lambda_{(2)}/\pi_{(2)}^-$	PHENIX [20, 21]	$0.072 \pm 0.017$	$0.068 \pm 0.016$	$0.074 \pm 0.017$
$\langle K^{*0} \rangle / \pi_{(2)}^-$	STAR [17, 24]	$0.039 \pm 0.011$		
$\phi/\pi_{(2)}^-$	STAR [17, 27]	$0.022 \pm 0.003$	$0.021 \pm 0.004$	$0.022 \pm 0.004$
$\Xi_{(2)}^-/\pi_{(2)}^-$	STAR [17, 28, 29]	$0.0093 \pm 0.0012$	$0.0072 \pm 0.0011$	$0.0060 \pm 0.0008$
$\Omega^-/\pi_{(2)}^-$	STAR [17, 28, 29]	$0.0014 \pm 0.0004$		

$\pi_{(2)}^\pm$  : includes 50% of pions from decays of  $\Omega$ ,  $\Xi$ ,  $\Sigma$ ,  $\Lambda$  and their anti-particles  
 $K_{(2)}^\pm$  : includes 100% of kaons from  $\phi$  decay  
 and 50% of kaons from  $\Omega$  and  $\bar{\Omega}$  decay  
 $K_s^0$  : includes 100% of  $K_s^0$  from  $\phi$  decay  
 $p_{(2)}$  and  $\bar{p}_{(2)}$  : includes 100% of protons from the decay of  $\Lambda$ ,  $\Sigma^0$  and their anti-particles  
 $\Lambda_{(2)}$  and  $\bar{\Lambda}_{(2)}$  : includes 100% of the contribution from the decay of  $\Xi$ ,  $\Omega$   
 and their anti-particles  
 $\Xi_{(2)}^-$  and  $\bar{\Xi}_{(2)}^+$  : includes 50% of the contribution from  $\Omega$  and  $\bar{\Omega}$  decay

As seen in Table I, in some cases the same ratios are at our disposal from various experiments. We include these multiply given ratios in our analysis as separate data points to be fit.

## V. RESULTS

### A. Centrality dependence of thermal parameters

The global results of the fits are displayed in Fig. 1. As is evident from Fig. 1a, the chemical freeze-out temperature is roughly constant at around 165  $MeV$  in Fit I. While the strangeness chemical potential is fairly flat at  $\mu_s \approx 10 MeV$  (with 10% variation, Fig. 1c), the baryon chemical potential (Fig. 1b) increases slightly with participant number in the range 33.4  $MeV$  to 38.5  $MeV$  (a 14% increase) in Fit I. Most striking, however, and the main result of our analysis, is the increase in strangeness saturation (Fig. 1d) with increasing centrality for all fit types. This confirms previous arguing [12, 15]. On a quantitative level, an analysis based on too few hadron species delivers non-reliable results, in particular also for  $\gamma_s$  (see Fig. 1d, Fit IV). Fits I and II, in contrast, deliver consistent results. Since we consider the phenomenologically introduced parameter  $\gamma_s$  as one possible indicator of deviations from equilibrium, the conclusion is that in central collisions equilibrium conditions for describing the chemical freeze-out are appropriate, while more peripheral collisions point to some off-equilibrium effects.

To highlight the role of the parameter  $\gamma_s$  on the quality of the data fits, we exhibit in Fig. 2 the  $\chi^2$  contours for fixed values of  $\gamma_s$  in the  $T - \mu$  plane. For definiteness,

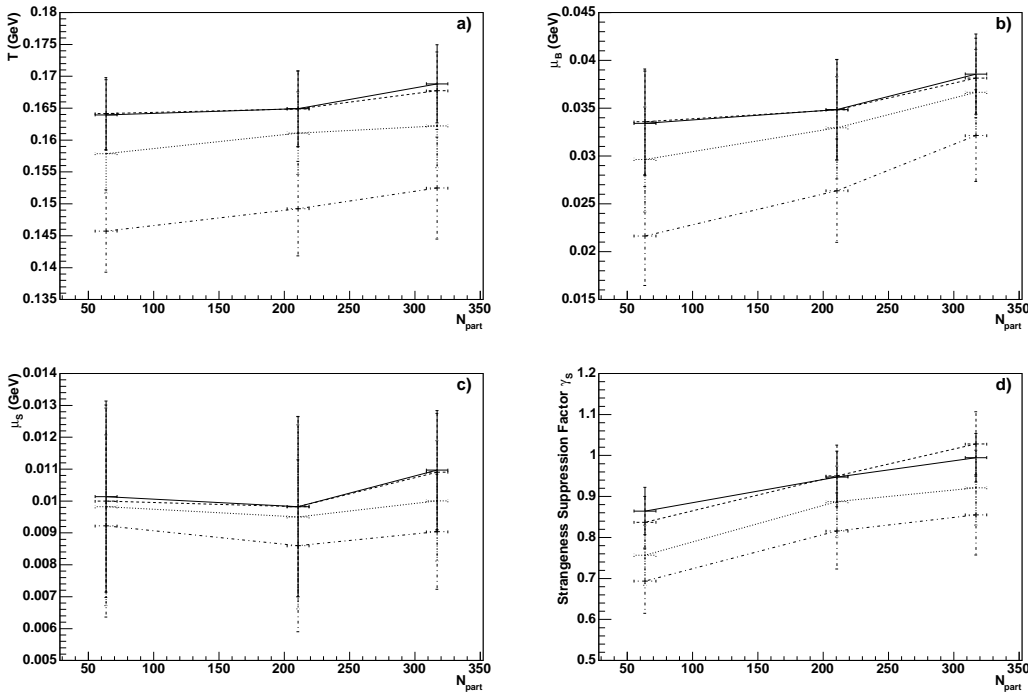


FIG. 1: The thermal parameters (a: temperature  $T$ , b: baryon chemical potential  $\mu_B$ , c: strangeness chemical potential  $\mu_s$ , d: strangeness saturation factor  $\gamma_s$ ) as extracted from the experimental data for the various fit types (Fit I: solid, Fit II: dashed, Fit III: dotted, Fit IV: dash-dotted curves).

only results for Fit I and peripheral collisions are shown. We have selected  $\gamma_s = 1$  (representing the assumption of full equilibrium), 0.85 (the optimum choice) and 0.5 (as rather extreme choice), respectively. The corresponding  $\chi^2/d.o.f$  are 24.1/12, 17.2/11 and 62.0/12. The figure evidences that lowering  $\gamma_s$  noticeably shifts  $T$  up, while the up-shift of  $\mu_B$  is less pronounced. The change in  $\chi^2/d.o.f$  quantifies the relevance of the parameter  $\gamma_s$  for the fits.

## B. Detailed comparison with data

After discussing the global trends, it is worthwhile to look into details. Instead of displaying the usual comparison of model results with data in one plot we consider each ratio individually to exhibit the centrality systematics.

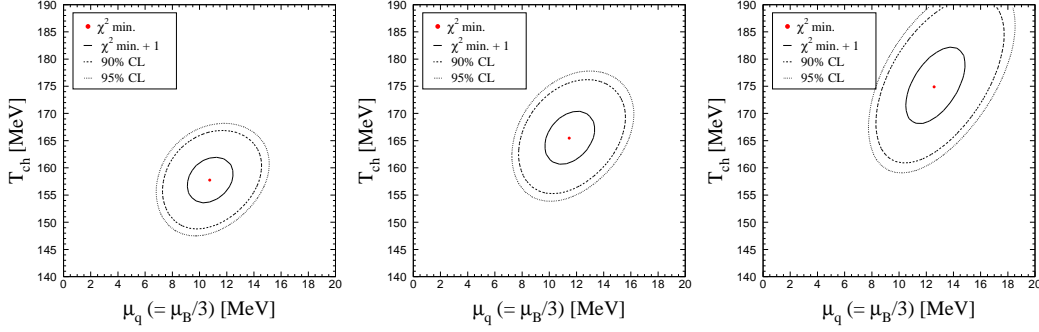


FIG. 2:  $\chi^2$  contours from Fit I of peripheral data.  $\gamma_s = 1$  (0.5) in left (right) panel. In the middle panel,  $\gamma_s = 0.85$  being the optimum choice.

### 1. Particle-anti-particle ratios

Fig. 3 summarizes such a comparison for the three centrality classes for the particle-anti-particle ratios. The data used from Table I are shown together with our model results.

For a qualitative understanding one can use the Boltzmann approximation ignoring widths. (At RHIC energies the use of Boltzmann statistics introduces errors in primordial yields at the level of 10% for pions, 1.3-1.5% for kaons and less than one percent for all other hadrons. Thus, given the intrinsic systematic uncertainties inherent in any thermal model analysis owing to the poorly constrained particle properties of the heavy resonances, quantum statistics is important only for pions.) The primordial density of hadron species  $i$  is then given by

$$n_i = \frac{g_i}{(2\pi^2)} \gamma_S^{|S_i|} m_i^2 T K_2(m_i/T) \exp(\mu_i/T). \quad (5.1)$$

Thus, the ratio of particle to anti-particle primordial yields is simply,

$$\frac{n_i}{n_{\bar{i}}} = \exp(2\mu_i/T). \quad (5.2)$$

Anti-particle-to-particle ratios therefore fix  $\mu_{B,S}/T$ . We note that these ratios are only slightly affected by feed-down (using the central Fit I best-fit parameters the percentage influence of feed-down is  $\pi_{(2)}^-/\pi_{(2)}^+$ : 1.0%,  $K_{(2)}^+/K_{(2)}^-$ : 2.9%,  $\bar{p}_{(1)}/p_{(1)}$ : 0.5%,  $\bar{p}_{(2)}/p_{(2)}$ : 3.7%,  $\bar{\Lambda}_{(1)}/\Lambda_{(1)}$ : 0.7%,  $\bar{\Lambda}_{(2)}/\Lambda_{(2)}$ : 4.2%,  $\bar{\Xi}_{(2)}^+/\Xi_{(2)}^-$ : 0.08%, and  $\bar{\Omega}/\Omega$ : 0%). Thus, the trends in these ratios translate directly into trends in  $\mu_S/T$  and  $\mu_B/T$ , while they are roughly insensitive to  $\gamma_S$  and  $T$ .

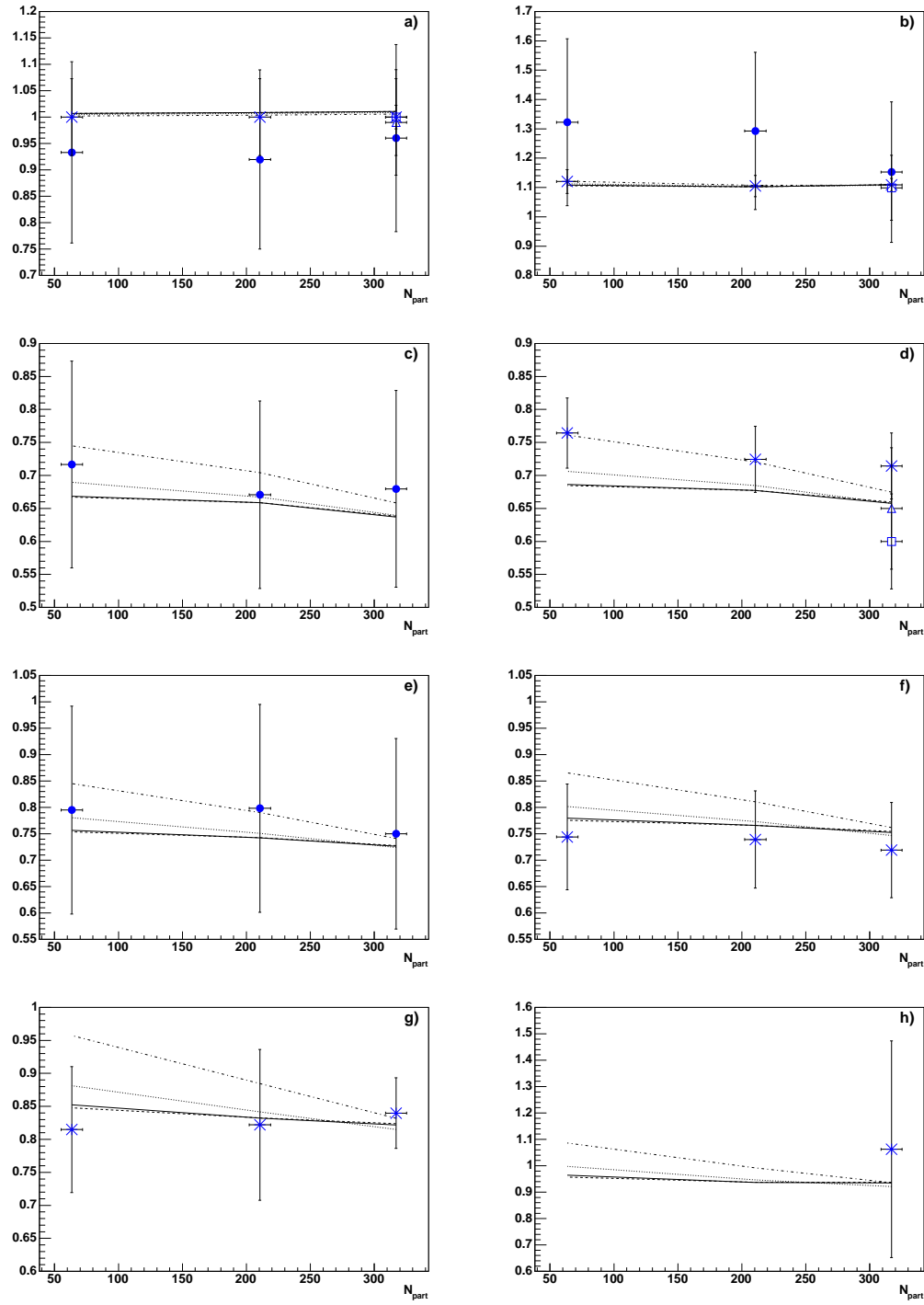
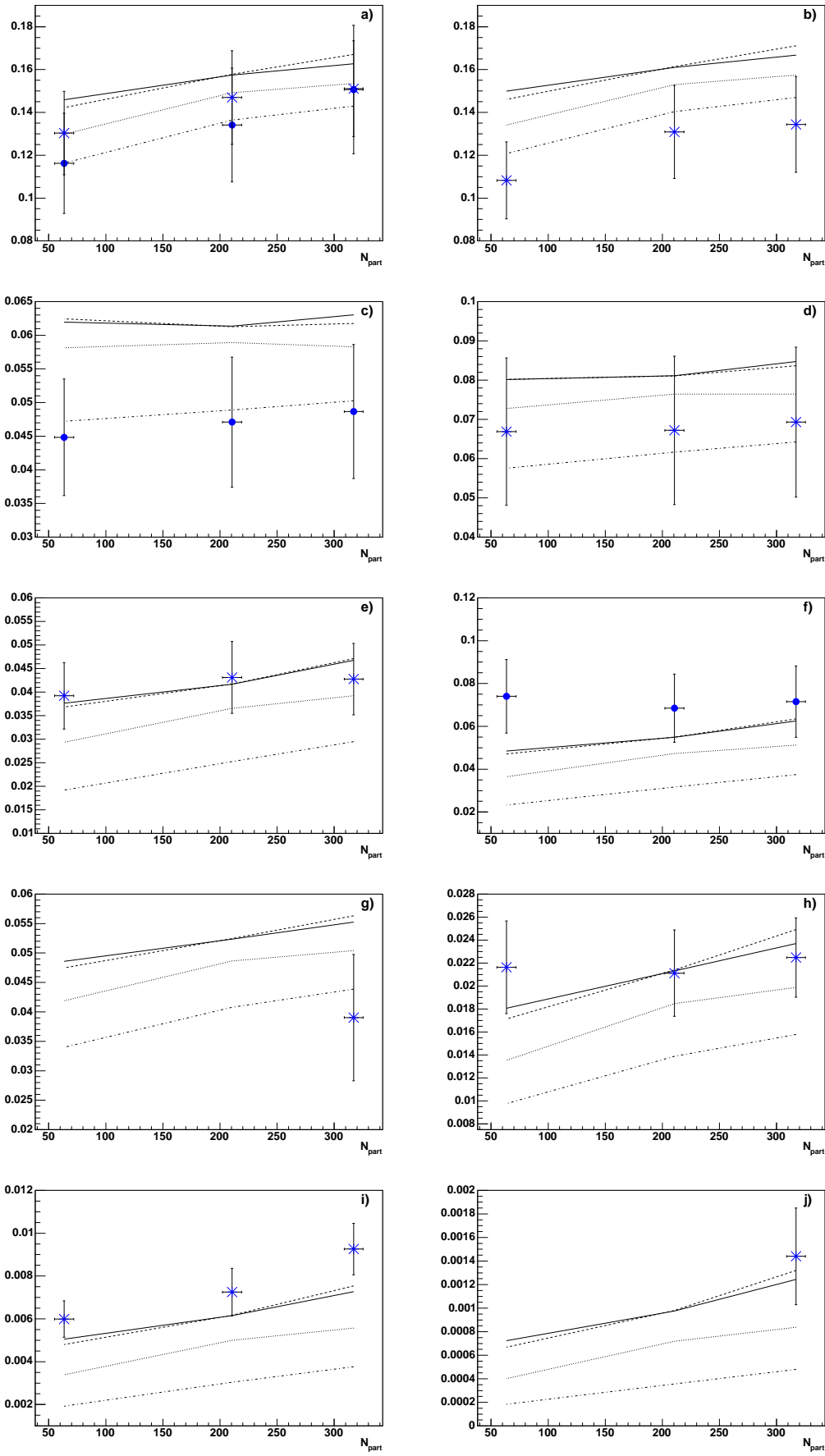


FIG. 3: Comparison between experiment and model results for particle-anti-particle ratios

(a:  $\pi_{(2)}^-/\pi_{(2)}^+$ , b:  $K_{(2)}^+/K_{(2)}^-$ , c:  $\bar{p}_{(1)}/p_{(1)}$ , d:  $\bar{p}_{(2)}/p_{(2)}$ , e:  $\bar{\Lambda}_{(1)}/\Lambda_{(1)}$ , f:  $\bar{\Lambda}_{(2)}/\Lambda_{(2)}$ , g:  $\bar{\Xi}_{(2)}^+/\Xi_{(2)}^-$ , h:  $\bar{\Omega}^+/\Omega^-$ ). Line codes as in Fig. 1, experimental results: STAR: stars, PHENIX: circles, PHOBOS: squares, BRAHMS: triangles, cf. Table I.



Let us now consider the individual ratios and begin with  $\pi_{(2)}^-/\pi_{(2)}^+$ . The experimental ratio is consistent with being flat and slightly below or equal to unity, while our model yields a  $\pi^-/\pi^+$  ratio slightly above 1 (see Fig. 3a). Model and experiment, however, agree within errors. There is no significant difference between the results of the four fits. Setting  $\mu_Q = 0$  drives the model ratio to very close to 1; deviations are due to feeding (since  $\mu_B$  and  $\mu_S$  are both greater than zero). With only strong decays included, the ratio is less than 1. Therefore it is the influence of the weak decays that pushes the ratio above 1. This ratio is insensitive to  $\mu_S$  and  $\mu_B$ : with a 5 *MeV* change in  $\mu_B$  the ratio varies by 0.2%, while a 5 *MeV* change in  $\mu_S$  leads to a 0.3% change in the ratio. A 0.2 change in  $\gamma_S$  furthermore affects the ratio by only 0.2%, while a 5 *MeV* change in  $T$  leads to only a 0.06% change in the ratio. Therefore, this ratio fixes nothing, and serves just as the motivation for setting  $\mu_Q = 0$ .

The ratio  $K_{(2)}^+/K_{(2)}^-$  is above 1 (see Fig. 3b) and drives  $\mu_S$  to positive values. Due to their much smaller errors, the STAR ratios are heavily weighted in the fit. This contributes to  $\mu_S$  having a slight kink as seen in Fig. 1c. The effect of the above-quoted feeding accounts for the slightly different shape of the  $K^+/K^-$  ratio compared with the  $\mu_S/T$  trend which can be deduced from Fig. 1. With this ratio removed from the fit,  $\mu_S/T$  would increase steeply with centrality, driven by the corrected  $\bar{\Lambda}/\Lambda$  to  $\bar{\Xi}^+/\Xi^-$  double ratio. This gives  $\bar{\Xi}^+/\Xi^-$  an increasing trend. In order to keep the  $\bar{\Lambda}/\Lambda$  ratio flat,  $\mu_B/T$  then similarly increases which causes  $\bar{p}/p$  to drop. Therefore, the kaon ratio is what keeps  $\mu_S$  flattish and gives it the ‘kink’.

The  $\bar{p}/p$  experimental ratios differ noticeably (see Fig. 3c and Fig. 3d), with STAR being the highest. These STAR data points are favored in fits since they have much reduced errors (consistently a factor of 3 less than those of PHENIX). These STAR ratios, however, are too high if the STAR  $\bar{\Lambda}/\Lambda$  ratio is to be simultaneously reproduced by the model (STAR  $\bar{p}/p$  supports a lower  $\mu_B$  as is seen when the  $\Lambda$ ’s are removed from the fit, as done in Fit IV). With  $\Lambda$ ’s excluded, the much smaller STAR errors lead to these  $\bar{p}/p$  data points being strongly favored in the mid-central and peripheral fits. This leads to a strong increase of  $\mu_B$  with centrality. Since the experimental  $\bar{\Lambda}/\Lambda$  ratio (Fig. 3e and f) is flattish, they support a similar behavior for  $\mu_B/T$  and  $\mu_S/T$ .

Excluding all but the STAR  $\bar{p}/p$  points in the most central bin removes the strong increase in  $\mu_B$  from the mid-central to central bins seen in Fit IV. Our suspicion that it is  $\bar{p}/p$  which causes  $\mu_B$  to increase is confirmed by repeating the fits with only anti-particle-to-particle ratios included (i.e., all particle-to-pion ratios excluded). Since these ratios are insensitive to  $\gamma_S$ , and  $T$  enters only together with the chemical potentials, in these reduced fits we fixed  $\gamma_S = 1$  and  $T = 165\text{ MeV}$  (both reasonable in light of the full results). The approximate trends in  $\mu_S/T$  and  $\mu_B/T$  observed in the full fits were reproduced using just these ratios. With the  $\bar{p}/p$  ratio excluded, the steady increase in  $\mu_B$  disappears; instead  $\mu_B/T$  decreases similarly to  $\mu_S/T$  as driven by the flatness in the  $\bar{\Lambda}/\Lambda$  ratio.

The ratio  $\bar{\Xi}^+/\Xi^-$  (see Fig. 3g) depends strongly on  $\mu_S/T$  and  $\mu_B/T$  and is little affected by feed-down. Similar fractional errors to the uncorrected  $\bar{\Lambda}/\Lambda$  ratio means both are treated equally in fits.

Although consistent within errors, the model trend decreases slightly with centrality, while the data are consistent with a weak increase. Comparing this experimental ratio with  $\bar{\Lambda}/\Lambda$ , the  $\bar{\Xi}^+/\Xi^-$  to  $\bar{\Lambda}/\Lambda$  double ratio increases. Thus,  $\mu_S/T$  is driven up particularly from the mid-central to central bin. As mentioned earlier, the  $K^+/K^-$  ratio leads to a kink in the trend for  $\mu_S$ . This effect wins over the influence of the  $\Xi$  to  $\Lambda$  double ratio which suggests an increase in  $\mu_S/T$ .

Unfortunately there is no centrality information on the ratio  $\bar{\Omega}^+/\Omega^-$ . Such data would allow even better determination of  $\mu_S$ . As seen in Fig. 3h, our model results agree fairly well with the data for the central bin.

## 2. Particle-to-pion ratios

The particle-to-pion ratios read in the Boltzmann approximation neglecting width

$$\frac{n_i}{n_\pi} = \gamma_S^{|S_i|} \frac{g_i}{g_\pi} \frac{m_i^2}{m_\pi^2} \frac{K_2(m_i/T)}{K_2(m_\pi/T)} \frac{\exp(\mu_i/T)}{\exp(\mu_\pi/T)}, \quad (5.3)$$

i.e., qualitatively, mixed particle ratios allow the determination of  $\gamma_S$  and  $T$ , and hence the  $\mu$ 's independently. Whereas the particle-to-anti-particle ratios feature just the combination  $\mu/T$ , the primordial particle-to-pion ratios feature also  $T$  in the combination  $K_2(m_i/T)/K_2(m_\pi/T)$ . This allows the temperature to be fixed

and then, given the values of  $\mu/T$  fixed by the particle-to-anti-particle ratios, the chemical potentials are determined. However, feed-down plays an important role in these ratios, so that the final observed ratios differ from the ratios of primordial densities quite substantially. This makes a detailed analysis of the influence of these ratios on the parameters much more difficult than in the case of the particle-to-anti-particle ratios. In fact, for the best-fit parameters corresponding to Fit I of the central bin, more than 70% of  $\pi^+$ 's come from decays.

A simple analysis shows how the ratio  $K_2(m_i/T)/K_2(m_\pi/T)$  varies with temperature for a number of hadron species  $i$ : Lowering the temperature has the effect of bringing the particle-to-pion ratios down. Furthermore, the fractional effect of changing the temperature is greater for the heavier particles.

After these general remarks let us consider in some detail the comparison of our model with data. The ratio  $K_{(2)}^-/\pi_{(2)}^-$  (Fig. 4a) is reasonably well reproduced in the fits. Since the errors on the PHENIX and STAR experimental ratios are similar, neither is heavily biased in the fit. The PHENIX data rise more rapidly than the STAR data (especially from the mid-central to central bin). Since the particle-to-anti-particle ratios support a centrality-independent  $\mu_S/T$ , the experimental  $K^-/\pi^-$  ratios drive an increase in strangeness saturation, with the PHENIX data supporting a steeper increase in  $\gamma_S$  than the STAR data (see Fig. 1d). In Fit I and II  $K^-/\pi^-$  is over-predicted. In contrast, the uncorrected  $\Lambda/\pi^-$  and  $\Xi^-/\pi^-$  are under-estimated (small fractional errors on  $\Xi^-/\pi^-$  mean that this ratio strongly influences the fit). With the  $\Xi$ 's removed in Fit III the STAR  $K^-/\pi^-$  data are well reproduced owing to the drop in  $T$  and  $\gamma_S$ . The big drop in this ratio when  $\Lambda$ 's are excluded from the fit is due to the further drop in  $\gamma_S$  and  $T$  in Fit IV seen in Fig. 1. The effect of this drop is somewhat lessened by the accompanying drop in  $\mu_S/T$  in the central and mid-central bins. Furthermore, the kaon to pion ratios are least affected by the temperature change in Fit IV.

The increase in the ratio  $K_S^0/\pi^-$  with centrality (Fig. 4b) also drives  $\gamma_S$  to increase. In the full fits (Fits I - III) it is somewhat over-estimated (a similar result is found in [15]), while the exclusion of the  $\Lambda$ 's (Fit IV) results in much better agreement. This is owing to the reduced  $\gamma_S$  in Fit IV. Comparing the results for the ratios  $K^-/\pi^-$  and  $K_S^0/\pi^-$  in Figs. 4a and b one gets the impression that the

PHENIX  $K^-/\pi^-$  data is compatible with STAR's  $K_S^0/\pi^-$  data, while the good fit in Fit III of STAR's  $K^-/\pi^-$  data result in a ratio  $K_S^0/\pi^-$  being at the upper limits of the error bars from STAR. The central  $\langle K^{*0} \rangle / \pi^-$  ratio reproduction by the model (Fig. 4g) follows the same trend as the  $K_S^0$ .

Let us now focus on the  $\bar{p}/\pi^-$  and  $\Lambda/\pi^-$  ratios (Figs. 4c, d, e and f). While the  $\bar{p}/\pi^-$  ratio is over-estimated by the model in Fits I - III,  $\Lambda/\pi^-$  is under-estimated except for the corrected  $\Lambda/\pi^-$  in the central bin in Fits I and II. With  $\Lambda$  excluded,  $\bar{p}/\pi^-$  is well reproduced, while  $\Lambda/\pi^-$  is greatly underpredicted. Therefore,  $\bar{p}/\pi^-$  drives  $T$  down, while  $\Lambda/\pi^-$  tends to raise  $\gamma_S$  and  $T$ .

The flatness of the ratio  $\phi/\pi^-$  (Fig. 4h) supports a centrality-independent  $\gamma_S$ . In Fits I and II there is fair agreement with the model, while this ratio is greatly under-estimated in Fit IV owing to the greatly reduced  $\gamma_S$  and  $T$ . The increasing trend of the model results is due to the increase in  $\gamma_S$  with centrality and the fact that  $n_\phi \sim \gamma_S^2$ .

The increase of the ratio  $\Xi^-/\pi^-$  (Fig. 4i) drives  $\mu_B/T$  to increase as well as  $\gamma_S$ . On the other hand, it causes  $\mu_S/T$  to drop. Again there is fair agreement with the model in Fits I and II, while this ratio is greatly under-estimated in Fit IV.

There is fair agreement of our model results with the  $\Omega^-/\pi^-$  ratio (Fig. 4j) in the central bin in Fits I and II. However, with  $\Xi$  and  $\Lambda$  removed agreement worsens.

Our final conclusion is that Fits I - II give a quite satisfactory description of most ratios, with the exception of  $K_S^0/\pi^-$ ,  $\langle K^{*0} \rangle / \pi^-$  and corrected  $\bar{p}/\pi^-$ . For the  $\langle K^{*0} \rangle / \pi^-$  and  $\Omega^-/\pi^-$  there are no data for mid-central and peripheral collisions. Thus our results may serve as predictions.

### C. Summary

In summary, we present an analysis of the centrality dependence of thermal parameters deduced from hadron multiplicities within a statistical-thermal model. The grand-canonical formalism is employed with quantum statistics and resonance widths included for all of the fits. We rely entirely on published data for the reaction Au + Au at  $\sqrt{s_{NN}} = 130$  GeV. Our aim is to employ the strangeness saturation factor  $\gamma_s$  as one possible indicator for deviations from equilibrium conditions in de-

scribing the chemical freeze-out. Indeed, for non-central collisions the systematic deviation of  $\gamma_s$  from unity can be considered as a hint to off-equilibrium effects, while for central collisions and using a sufficiently complete set of available multiplicity ratios at mid-rapidity there is no indication for deviations from equilibrium conditions.

We present a detailed comparison of the model results with data. The trends in  $\mu_{B,S}/T$  are fixed by the anti-particle-to-particle ratios. The  $K^+/K^-$  ratio is responsible for keeping  $\mu_S/T$  essentially flat. This wins over the influence of the  $\Xi$  to  $\Lambda$  double ratio which tends to increase  $\mu_S/T$ . The  $\bar{p}/p$  ratio drives  $\mu_B/T$  up, which wins over  $\bar{\Lambda}/\Lambda$ 's attempts to make  $\mu_S/T$  and  $\mu_B/T$  behave similarly. The temperature and strangeness saturation are fixed by the particle-to-pion ratios. The observed increase in  $\gamma_s$  is driven predominantly by the increase in the  $K^-/\pi^-$  ratio and the flatness of  $\mu_S/T$  as fixed by the  $K^+/K^-$  ratio.

A possible extension of the present work is the analysis of saturation in the non-strange sector, parameterized by  $\gamma_q$  being a factor similar to  $\gamma_s$  [31]. Since our fits to the data deliver reasonably small values of  $\chi^2$  we believe, however, that there is not too much room left for sizeable deviations of  $\gamma_q$  from unity. This issue deserves a separate investigation. More tempting is the analysis of data for  $\sqrt{s_{NN}} = 200 \text{ GeV}$ . The explorative study in [15] points to a similar behavior of  $\gamma_s$  as we find for  $\sqrt{s_{NN}} = 130 \text{ GeV}$ . Even more interesting is to test heavy flavor production; due to their larger intrinsic masses, heavy flavors should have a higher sensitivity to the medium. In particular, hadrons with open and hidden charm may require a corresponding factor  $\gamma_c$ .

### Acknowledgments

This work has been supported in part by the National Research Foundation of South Africa, the U.S. Department of Energy under Contract No. DE-AC03-

76SF00098 and the German BMBF grant 06DR121.

---

- [1] P. Braun-Munzinger, K. Redlich, J. Stachel, nucl-th/0304013 in *Quark-Gluon Plasma 3*, (eds.) R. Hwa, X.N. Wang; K. Redlich, J. Cleymans, H. Oeschler and A. Tounsi, Acta Phys. Polonica B 33 (2002) 1609; J. Letessier, J. Rafelski, Int. J. Mod. Phys. E 9 (2000) 107.
- [2] F. Becattini, J. Cleymans, A. Keränen, E. Suhonen, K. Redlich, Phys. Rev. C 64 (2001) 024901.
- [3] P. Braun-Munzinger et al., Phys. Lett. B 344 (1995) 43, B 365 (1996) 1, B 465 (1999) 15, B 518 (2001) 41.
- [4] J. Cleymans, K. Redlich, Phys. Rev. Lett. 81 (1998) 5284, J. Sollfrank, J. Phys. G: Nucl. Part. Phys. 23 (1997) 1903.
- [5] J. Cleymans, K. Redlich, Phys. Rev. C 60 (1999) 054908.
- [6] W. Florkowski, W. Broniowski, Phys. Rev. C 65 (2002) 064905, Phys. Rev. Lett. 87 (2001) 272302; F. Becattini, G. Passaleva, Eur. Phys. J. C 23 (2002) 551.
- [7] P. Braun-Munzinger, J. Stachel, C. Wetterich, Phys. Lett. B 596 (2004) 61.
- [8] T. Biro, B. Müller, Phys. Lett. B 578 (2004) 78; A. Majumder, V. Koch, Phys. Rev. C 68 (2003) 044903.
- [9] P. Koch, B. Müller, J. Rafelski, Phys. Rep. 142 (1986) 167; J. Letessier, J. Rafelski, A. Tounsi, Phys. Rev. C 50 (1994) 405; C. Slotta, J. Sollfrank, U. Heinz, AIP Conf. Proc. (Woodbury) 340 (1995) 462.
- [10] F. Becattini, M. Gazdzicki, A. Keränen, J. Manninen, R. Stock, Phys. Rev. C 69 (2004) 024905; I.G. Bearden et al. (NA44), nucl-ex/0202019; F. Becattini, M. Gazdzicki, J. Sollfrank, Eur. Phys. J. C 5 (1998) 143.
- [11] J. Cleymans, B. Kämpfer, S. Wheaton, Phys. Rev. C 65 (2002) 027901.
- [12] J. Cleymans, B. Kämpfer, S. Wheaton, Nucl. Phys. A 715 (2003) 553c; J. Cleymans, B. Kämpfer, P. Steinberg, S. Wheaton, hep-ph/0212335, J. Phys. G 30

(2004) S595;

B. Kämpfer, J. Cleymans, K. Gallmeister, S. Wheaton, hep-ph/0202134, *Acta. Phys. Hung. New Ser. Heavy Ion Phys.* 18 (2003) 1.

[13] D. Zschiesche, S. Schramm, J. Schaffner-Bielich, H. Stöcker, W. Greiner, *Phys. Lett. B* 552 (2002) 7.

[14] K. Hagiwara et al., *Phys. Rev. D* 66 (2002) 010001.

[15] M. Kaneta, N. Xu, nucl-th/0405068.

[16] F. Becattini, *J. Phys. G* 28 (2002) 1553;  
 D. Magestro, *J. Phys. G* 28 (2002) 1745;  
 A. Baran, W. Broniowski, W. Florkowski, *Acta Phys. Pol. B* 35 (2004) 779.

[17] J. Adams et al. (STAR), nucl-ex/0311017;  
 M. Calderon de la Barca Sanchez, nucl-ex/0111004.

[18] C. Adler et al. (STAR), *Phys. Rev. Lett.* 89 (2002) 092301.

[19] I.G. Bearden et al. (BRAHMS), *Phys. Rev. Lett.* 87 (2001) 112305.

[20] K. Adcox et al. (PHENIX), *Phys. Rev. Lett.* 88 (2002) 242301.

[21] K. Adcox et al. (PHENIX), *Phys. Rev. Lett.* 89 (2002) 092302.

[22] B.B. Back et al. (PHOBOS), *Phys. Rev. Lett.* 87 (2001) 102301.

[23] C. Adler et al. (STAR), *Phys. Lett. B* 595 (2004) 143.

[24] C. Adler et al. (STAR), *Phys. Rev. C* 66 (2002) 061901.

[25] C. Adler et al. (STAR), *Phys. Rev. Lett.* 87 (2001) 262302.

[26] C. Adler et al. (STAR), *Phys. Rev. Lett.* 86 (2001) 4778.

[27] C. Adler et al. (STAR), *Phys. Rev. C* 65 (2002) 041901(R).

[28] J. Castillo et al. (STAR), *Nucl. Phys. A* 715 (2003) 518c.

[29] J. Adams et al. (STAR), *Phys. Rev. Lett.* 92 (2004) 182301.

[30] C. Suire et al. (STAR), *Nucl. Phys. A* 715 (2003) 470c.

[31] J. Lettesier, J. Rafelski, *Phys. Rev. C* 59 (1999) 947.

[32] Actually we use two independent codes with different upper limits of the employed hadronic mass spectrum. The corresponding differences in results are tiny. One of the codes is described in S. Wheaton, J. Cleymans, hep-ph/0407174.